The Research Council of Norway (NFR)

NORSAR

NORSAR Scientific Report No. 2-93/94

Semiannual Technical Summary

1 October 1993 – 31 March 1994

Kjeller, May 1994

7.3 Signal detection and waveform extraction in the coda of a strong, interfering event

Introduction

A possible scenario for evading a nuclear testing treaty is to hide the seismic signals from a nuclear explosion in the wavetrain of a strong interfering earthquake. At small aperture arrays, some improvement in detection and parameter estimation capability of such "hidden" signals can be obtained by conventional beamforming and filtering techniques. There are, however, other approaches that are likely to be more powerful for this purpose, and we have in this study investigated a number of such methods.

For simplicity and to avoid confusion, the "hidden" signal is in this paper called "the explosion", whereas the interfering wavetrain is called "the earthquake" or the "noise". In general, signal detection and waveform extraction in the coda of a strong interfering wavetrain can be performed under different conditions that arise in different applications:

1. The azimuths and slownesses of both the explosion and the earthquake signals are assumed to be known.
2. The azimuth and slowness of the explosion signal is known, but unknown for the earthquake, e.g., due to uncertainty of the azimuth and slowness characteristics of the earthquake coda or in the case of real time processing.
3. The azimuth and slowness of the earthquake is known, but unknown for the explosion.
4. The azimuth and slownesses are unknown for both the explosion and the earthquake.

In practical applications, scenarios 1 and 3 above would probably be the most useful. In these two cases, it is assumed that the earthquake has been well located, so that azimuth and slowness can be assumed known. The search for a potential hidden signals (the explosion) might be done without any assumptions on its location (case 3), or one might want to focus upon a site of special interest (case 1).

The scenarios 2 and 4 are most interesting for detecting potential hidden events relatively far into the coda of the earthquake. Even if the earthquake location is known, the scatter in azimuth and slowness of coda phases might make it appropriate to apply the model of an unknown earthquake source as done in these two cases.

In this paper we discuss array data processing algorithms that seem to be helpful to solve the problem under conditions 1) and 2). In these cases, the apparently best way to detect and estimate the parameters of the signal is to apply beamforming (or group filtering) procedures by which the array spatial receiver function attains its maximum gain in the direction and slowness of the explosion while minimizing the gain in the direction and azimuth of the interfering earthquake.

Spatial Rejection Filtering

When the azimuths and slownesses of both the explosion and the earthquake signals are known, we propose to use a "spatial rejection group filter" (SRGF) to improve the detection and parameter estimation capability of the "hidden" explosion. A group filter $\bar{r}(j) = (r_1(f), \ldots, r_m(f))$ is a multichannel filter that transforms the m input array data traces $\bar{x}(f) = (x_1(f), \ldots, x_m(f))^T$ (where T denotes transposition) into a scalar trace $y(f)$ via the equation

$$y(f) = \bar{r}^*(f)\,\bar{x}(f) \tag{1}$$

Equation (1) is written in the frequency domain, where f is the frequency $0 < f < f_{smp}/2$, f_{smp} is the sampling frequency and * denotes complex conjugation.

The vector frequency response of the spatial rejection group filter can be written as:

$$\bar{r}^*(f) = \frac{\bar{h}_s^*(f)\,\mathbf{B}(f)}{\bar{h}_s^*(f)\,\mathbf{B}(f)\,\bar{h}_s(f)} \tag{2}$$

where

$$\bar{h}_s(f) = e^{-i2\pi\tau_{s,k}f/f_{smp}}, \qquad k = 1, \ldots, m \tag{3}$$

is the columns vector of "signal frequency delays" corresponding to the signal time delays $\tau_{s,k}$ between the *1st* sensor and the *k-th* sensor of the array.

$$\mathbf{B}(f) = \frac{\mathbf{I} - \bar{h}_n(f)\,\bar{h}_n^*(f)}{\bar{h}_n^*(f)\,\bar{h}_n(f)} \tag{4}$$

(where **I** is the identity matrix) is the matrix spatial rejection filter designed to reject the purely coherent wave arriving from the direction and slowness of the interfering earthquake source (the "noise"). The matrix $\mathbf{B}(f)$ is determined by the "noise frequency delays"

$$\bar{h}_n(f) = e^{-i2\pi\tau_{n,k}f/f_{smp}}, \qquad k = 1, \ldots, m \tag{5}$$

corresponding to the time delays $\tau_{n,k}$ of the interfering earthquake signals.

For the problem under discussion, the residual beamforming (RB) method is often used (Gupta et al, 1990). By this method, the beam steered to the "noise" direction is subtracted from every channel to create residual traces. Then a new beam steered to the signal direction is composed from the residuals. This method can be formulated as the implementation of a group filtering procedure with the vector frequency response

$$\bar{r}_{RB}(f) = h_s^*(f)\,\mathbf{B}(f) \tag{6}$$

Both group filters (2) and (6) suppress (theoretically - completely eliminate) the interfering purely coherent "noise" wave arriving from the assigned direction. The array record of the interfering wave can be written in the frequency domain in the form $\bar{n}(f) = \bar{h}_n(f)\, n_{WF}(f)$, where $n_{WF}(f)$ is the (scalar) spectrum of the interfering wave.

Substituting $\bar{n}(f)$ into eq. (1) gives

$$z(f) = \bar{r}_{RJ}^{*}(f)\,\bar{n}(f) = 0 \quad \text{and} \quad z(f) = \bar{r}_{RB}^{*}(f)\,\bar{n}(f) = 0 \tag{7}$$

because

$$\mathbf{B}(f)\,\bar{n}(f) = \left[\frac{\bar{h}_n(f) - \bar{h}_n(f)\,\bar{h}_n^{*}(f)\,\bar{h}_n(f)}{\bar{h}_n^{*}(f)\,\bar{h}_n(f)}\right] n_{WF}(f) = 0 \tag{8}$$

Note that the RB method has a disadvantage because it distorts the frequency content of the "hidden" explosion signal, and can therefore not be regarded as "pure spatial" filtering. In contrast, the SRGF is a signal undistorting procedure. This is shown in the following:

The vector spectrum of an array record for a purely coherent "hidden" signal has the form $\bar{s}(f) = \bar{h}_s(f)\, s_{WF}(f)$, where $s_{WF}(f)$ is the scalar spectrum of the signal waveform. Substituting $\bar{s}(f)$ into eq. (1) gives for the SRGF method

$$y(f) = \frac{\bar{h}_s^{*}(f)\,\mathbf{B}(f)\,\bar{h}_s(f)\,s_{WF}(f)}{\bar{h}_s^{*}(f)\,\mathbf{B}(f)\,\bar{h}_s(f)} = s_{WF}(f) \tag{9}$$

For the RB method

$$y(f) = \bar{h}_s^{*}(f)\,\mathbf{B}(f)\,\bar{h}_s(f)\,s_{WF}(f) = \bar{h}_s^{*}(f)\left[\frac{\bar{h}_s(f) - \bar{h}_n(f)\,\bar{h}_n^{*}(f)\,\bar{h}_s(f)}{\bar{h}_n^{*}(f)\,\bar{h}_n(f)}\right] s_{WF}(f) \tag{10}$$

$$= \bar{h}_s^{*}(f)\,\bar{\rho}_s(f)\,s_{WF}(f)$$

To illustrate the difference in performance between the spatial rejection group filter (SRGF) and the residual beamforming (RB) methods, we have simulated a mixture of a two fully coherent plane waves with different azimuths and slownesses, using the sensors of the NORESS array. The signal plane wave was assumed to arrive from the Novaya Zemlya Test Site (azimuth: 32.9 deg., apparent velocity: 14.8 km/s), and the signal waveform was generated as a linear frequency modulated signal with constant amplitude ("sweep signal"). The interfering (noise) plane wave was assumed to arrive from the Hindu Kush area (azimuth: 101.0 deg., apparent velocity: 14.8 km/s), and its waveform was set equal to a real Hindu Kush P-phase observation. The ratio between the maximum amplitudes of the signal and the interfering plane wave was 0.13.

Fig. 7.3.1a shows the residuals after processing with the matrix spatial rejection filter **B**(f). We see that the interfering wave is completely suppressed, but the shape of the"hidden"

signal is distorted at low frequencies. We also note that distortions are different for the different channels.

The upper trace of Fig. 7.3.1b is the result of conventional beamforming steered to the Novaya Zemlya Test Site. In this case the low SNR hidden signal cannot be identified. The second trace of Fig. 7.3.1b is the result of the residual beamforming method realized as group filtering in the frequency domain in accordance with equations (1) and (6). The simulated interfering earthquake waveform is completely suppressed, but the "hidden" signal amplitude is strongly reduced at low frequencies. It follows from eq. (10) that these signal frequency distortions are dependent on both the array geometry and the arrival directions of the incoming signals. The third trace of Fig. 7.3.1b is the output of spatial rejection group filtering in accordance with equations (1) and (2). This group filter extracts the sweep signal from the interfering earthquake and retains the waveform of the hidden signal undistorted. The fluctuations of the signal amplitudes at the end of the trace are explained by signal frequencies approaching the Nyquist frequency of the data.

In practice, signals arriving at an array do not consist of a single plane wave component and are not fully coherent among the array sensors. To illustrate the performance of SRGF and RB under such "real" conditions, we have created an event mixture by superimposing down-scaled NORESS records of the Novaya Zemlya (NZ) explosion of 24 October 1990 in the coda of a real Hindu Kush (HK) earthquake (Origin time: Oct. 25, 1990, 04.53.59.9). The ratio between the maximum amplitudes of the explosion and the earthquake was 0.2, and the P-phase from the explosion was set to arrive 12 s after the HK P-arrival. The lower trace of Fig. 7.3.2 show the event mixture at the central element of the NORESS array. The top trace is the conventional beam steered in agreement with the delays of the NZ P-phase. Also in this case we can see that the output from the RB method (trace no. 3) contain less low frequency components for the hidden signal as compared to the output from the SRGF (trace no. 2). It should also be emphasized that high-pass filtering of the SRGF output will for the NZ P-phase provide SNR comparable to the SNR of the output from the RB method.

Adaptive Optimal Group Filtering

The late part of an earthquake coda consists of wave components arriving from very different azimuths and slownesses. To reject this type of interfering energy, it is not very meaningful to use the spatial rejection group filter. The same applies to real-time processing, when the frequency delays are unknown. In this situation (case 2 of the Introduction) the adaptive optimal group filter (AOGF) can be helpful (Kushnir et al., 1990a; Kushnir et al., 1990b). The vector frequency response of the AOGF filter is

$$\bar{r}_{AO}{}^{*}(f) = \frac{\bar{h}_s{}^{*}(f)\,\hat{\mathrm{F}}_n^{-1}(f)}{\bar{h}_s{}^{*}(f)\,\hat{\mathrm{F}}_n^{-1}(f)\,\bar{h}_s(f)} \tag{11}$$

where $\hat{\mathrm{F}}_n^{-1}(f)$ is an estimate of the inverse matrix spectral density of the array "noise" (in our case the "noise" is the interfering event). Kværna and Kushnir (1991) showed that the-

oretically an adaptation window could include the plane wave signal we wanted to retrieve without significantly degrading the performance of AOGF filtering. We will refer this type of adaptation as self-adaptation.

Fig. 7.3.3 presents the results from processing the mixture of simulated plane waves (described in the connection with Fig. 7.3.1b) using the self-adaptive AOGF. The upper trace is the result of conventional beamforming steered to the Novaya Zemlya Test Site. The second trace is the output from processing with the self-adapted AOGF and the third trace is the output from the SRGF (assuming signal from Novaya Zemlya and interfering energy from Hindu Kush). The bottom trace shows the mixture as observed on the central NORESS sensor. When comparing the second and the third trace we find that the self-adaptive AOGF in the case of two interfering plane waves performs almost as well as the spatial rejection group filter, and we emphasize that the self-adaptive AOGF does not require any information on the arrival direction of the interfering event.

However, our experiments with mixtures of real events revealed a significant reduction in the performance of the AOGF filtering when the self-adaptation was performed, as compared to adaptation to the interfering event without using the signal window. We believe that this is due to the fact that both the signal and the interfering energy deviate strongly from single plane wave components. We will in the following illustrate this problem:

In Fig. 7.3.4a, the adaptation of the AOGF was made using the pure Hindu Kush recording. The NZ signal was then mixed with the Hindu Kush event (SNR 0.1) and AOGF filtering was performed. The result is shown in traces 2 and 3, using two slightly different implementations of the algorithm. For comparison, the output from conventional beamforming and SRGF is shown in traces 1 and 4. For this artificial situation, the performance of AOGF is excellent. However, results from AOGF after self-adaptation do not give nearly as good results, see traces 2 and 3 of Fig. 7.3.4b. In Fig. 7.3.4c the SNR of the NZ signal was raised to 0.3, and we see that the both the output from AOGF after self-adaptation (traces 2 and 3) and SRGF shown in the lower trace, clearly extract the signals from the earthquake coda.

Adaptive Optimal Phase Detection

The difference in frequency content between the Novaya Zemlya explosion and the Hindu Kush earthquake may enable us to detect the explosion on the self-adapted AOGF trace even if the SNR is very small. Fig. 7.3.5 shows the result after processing the self-adapted AOGF output with an adaptive optimal phase detector (AOPD). The SNR of the NZ signal was set to 0.05, and the NZ P-phase arrived 21 sec after the Hindu Kush P-arrival. The entire self-adapted AOGF output (trace no. 3) was used for detector adaptation, resulting in an average AR-model. Then the AR-coefficients were used for calculation of the Chi-squared detector statistics (Pisarenko et al., 1987; Kushnir et al., 1991) using data within 4-sec windows moving along the self-adapted AOGF trace. The detector statistics are shown in the upper trace of Fig. 7.3.5. We see that although the explosion signal is not clearly identified on the output from the self-adapted AOGF (trace no. 3) or SRGF (trace no. 4), the AOPD (trace no. 1) gives us convincing evidence of the presence of the signal.

The high sensitivity of the AOPD can therefore be helpful as a tool to be used for signal detection and waveform extraction of signals with low SNR. A practical procedure would be first to run the AOPD on a conventional beam output to determine the approximate onset time of the signal. The second step would comprise AOGF adaptation using the interval before (and may be after) the signal arrival, and the final step would be to process the entire data segment with AOGF.

Fig. 7.3.6 illustrates the performance of such a combined procedure. A mixture of real Novaya Zemlya and Hindu Kush recordings with SNR 0.2 was created. The onset time of the Novaya Zemlya signal was set to 41 sec after the onset of the Hindu Kush P-arrival. The conventional beam steered to Novaya Zemlya is shown in the second trace, but the signal is difficult to identify. However, after running the AOPD, the presence of a signal is clear. After running AOGF adaptation on the time segment preceding the signal (0-39 sec.), the data segment (0-60 sec.) was filtered by AOGF (trace no. 3). We see that a clear signal waveform is extracted, and the quality is somewhat better than the output from SRGF shown in trace no. 4. In practice, the SRGF cannot be implemented when information on the interfering signal is unknown.

A. Kushnir, MITPAN, Moscow
T. Kværna

References

Gupta, I.N., C.S. Lynnes and R.A. Wagner (1990): Broadband F-k analysis of array data to identify sources of local scattering, *Geophys. Res. Letters*, 17, 2, 183-186.

Kushnir, A.F., V.M. Lapshin, V.I. Pinsky and J. Fyen (1990): Statistically optimal detection using small array data, *Bull. Seism. Soc. Am.*, 80, 6, 1934-1950.

Kushnir, A.F., V.I. Pinsky, S.L. Tsvang, J. Fyen, S. Mykkeltveit and F. Ringdal (1990): Optimal group filtering and noise attenuation for the NORESS and ARCESS arrays, *Semiann. Tech. Summ., 1 April - 30 September 1990*, NORSAR Sci. Rep. no. 1-90/91, Kjeller, Norway, 115-134

Kushnir, A.F., J. Fyen and T. Kværna (1991): Studying of multichannel statistical data processing algorithms in the framework of the NORSAR event processing package, *Semiann. Tech. Summ., 1 October 1990 - 31 March 1991*, NORSAR Sci. Rep. no. 2-90/91, 82-103.

Kværna, T. and A.F. Kushnir (1991): Initial testing of mixed event separation using statistically optimal adapative algorithm, *Semiann. Tech. Summ., 1 April - 30 September 1991*, NORSAR Sci. Rep. no. 1-91/92, 112-126.

Pisarenko, V.F., A.F. Kushnir and I.V. Savin (1987): Adaptive algorithms for estimation of onset moments of seismic phases, *Phys. Earth Planet. Inter.*, 47, 4-10.

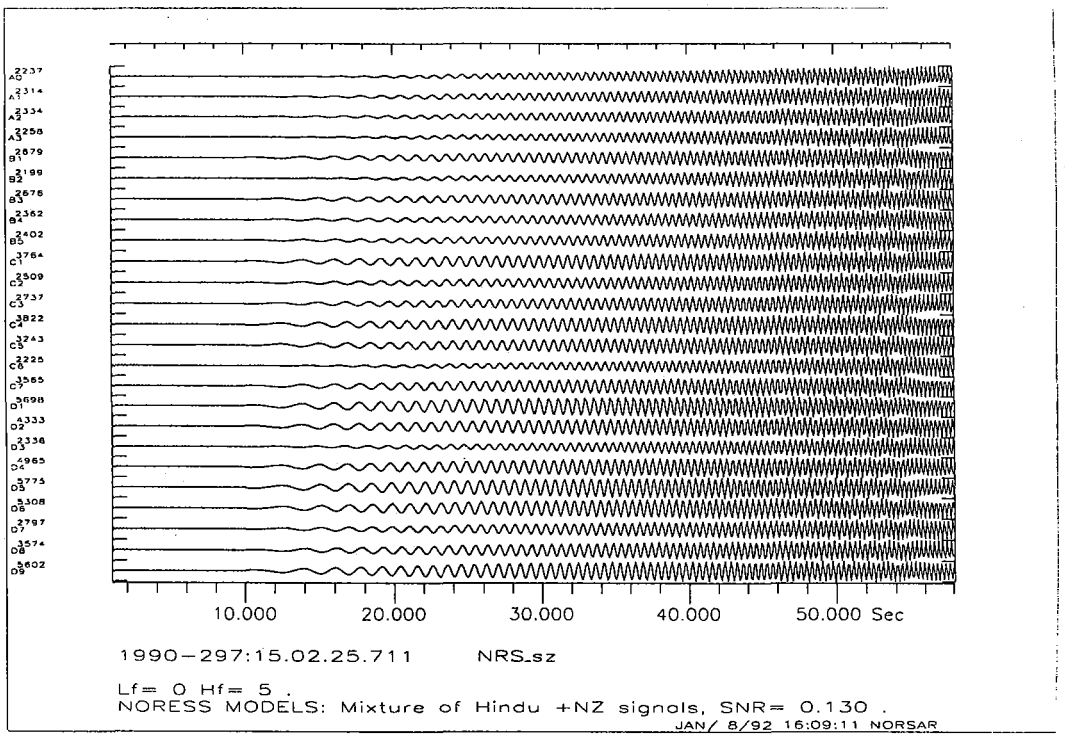

Fig. 7.3.1a. Residuals after processing a simulated mixture of two plane waves with a matrix spatial rejection filter. See text for a detailed explanation.

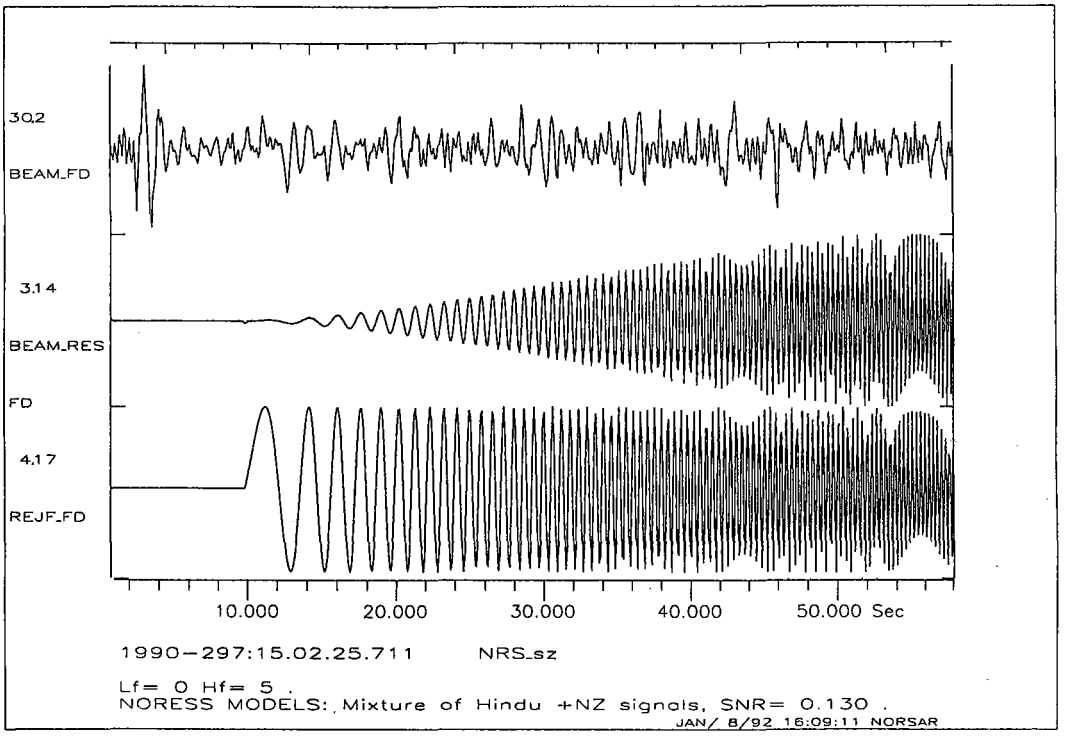

Fig. 7.3.1b. Results after processing a simulated mixture of two plane waves with three different rejection filters. The upper trace - conventional beamforming, the second trace - residual beamforming, the third trace - spatial rejection group filter. See text for detailed explanation.

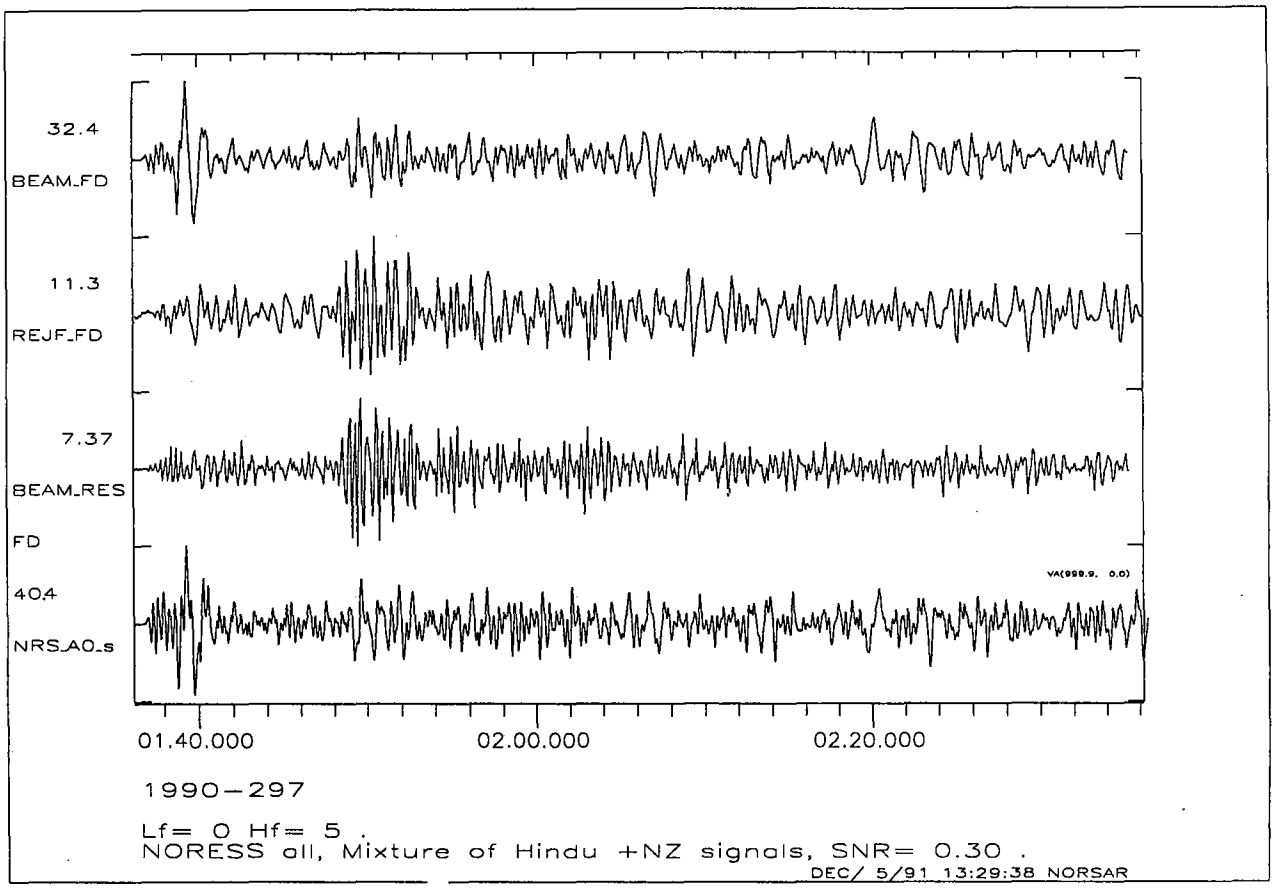

Fig. 7.3.2. Output after processing an artificial mixture of two NORESS recorded events with the spatial rejection filters.The upper trace - conventional beamforming, the second trace - spatial rejection group filter, the third trace - residual beamforming. The lower trace shows the event mixture at the central element of the NORESS array. See text for detailed explanation.

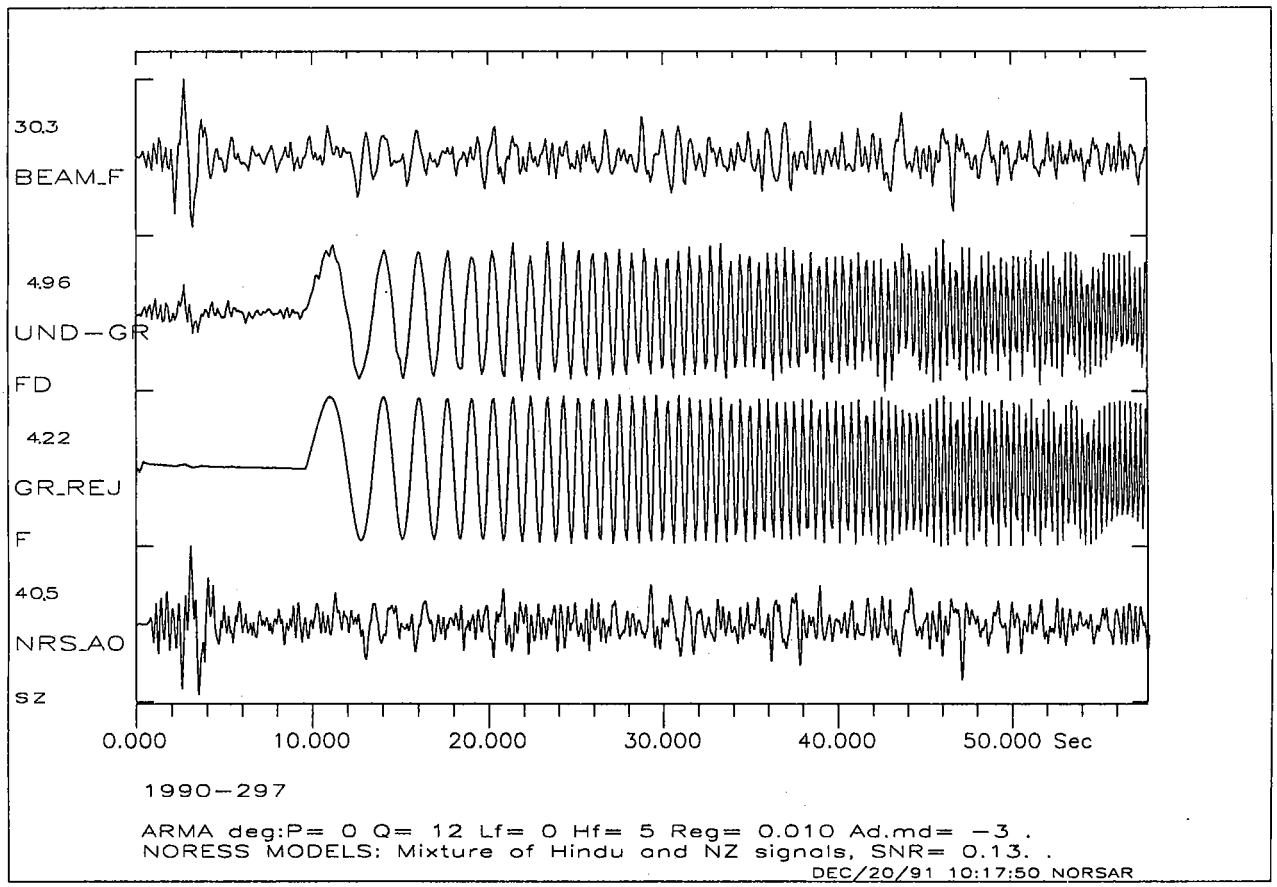

Fig. 7.3.3. Trace no. 2 shows the output after processing a simulated mixture of two plane waves with the self-adaptive optimal group filter. Trace no. 1 is the output after conventional beamforming, and trace no. 3 shows the output of the spatial rejection group filter. The lower trace shows the mixture at the central element of the NORESS array. See text for detailed explanation.

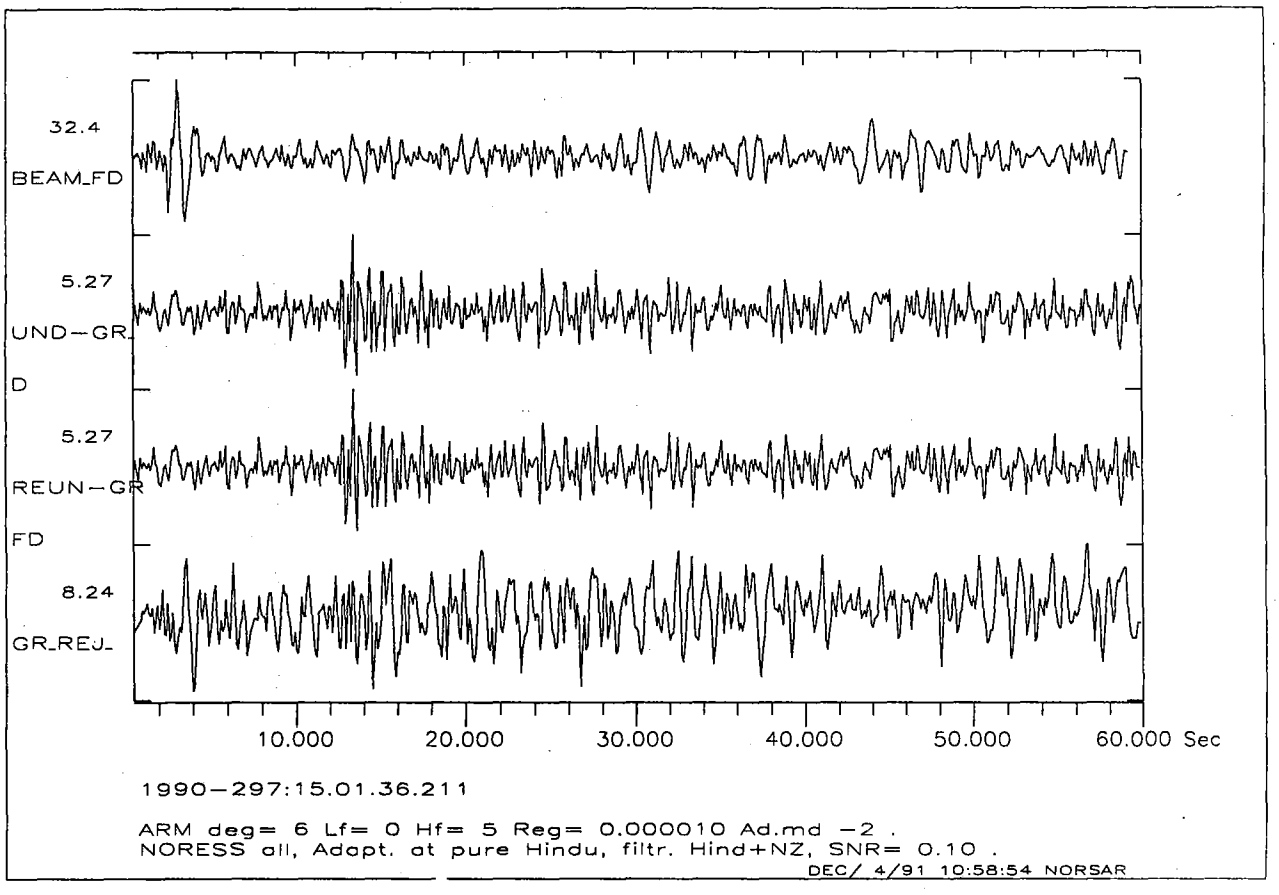

Fig. 7.3.4a. Figure illustrating the performance of the adaptive optimal group filter for separating an artificial event mixture. In this "unreal" implementation, the wanted signal (arriving at about 13 seconds) was not included in the adaptation. Traces no. 2 and no. 3 show outputs from the adaptive optimal group filter, using two slightly different implementations of the method. Trace no. 1 is the output after conventional beamforming, and trace no. 4 shows the output of the spatial rejection group filter. It is clear that in this "theoretically ideal" situation the adaptive optimal group filter has an excellent performance. See text for more details.

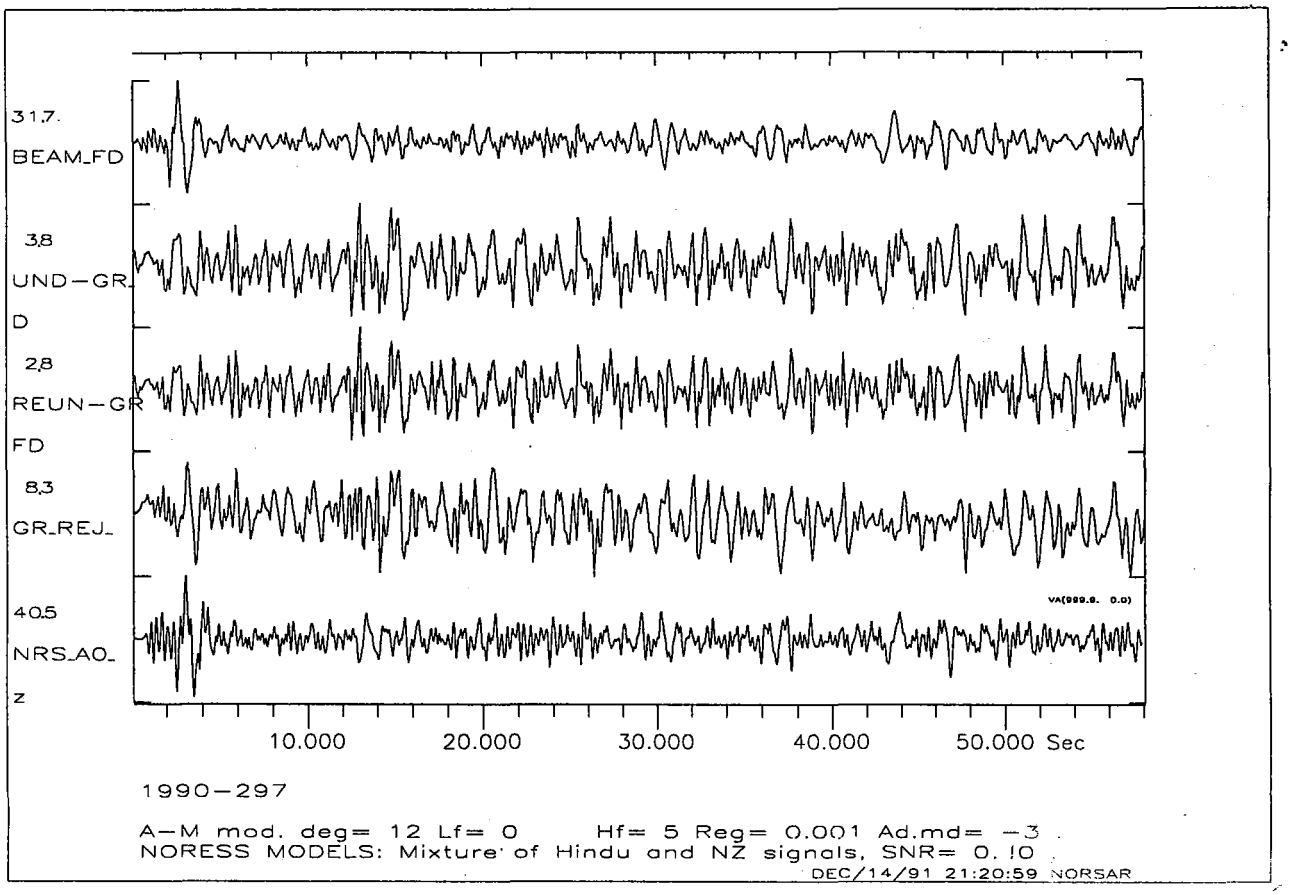

Fig. 7.3.4b. Figure illustrating the performance of the self-adaptive optimal group filter for separating an artificial event mixture. Traces 1-4 correspond to traces 1-4 of Fig. 7.3.4a. We believe that the degradation in performance relative to results shown in Fig. 7.3.4a is due to fact that both the signal and the intefering energy deviate strongly from single plane wave components.

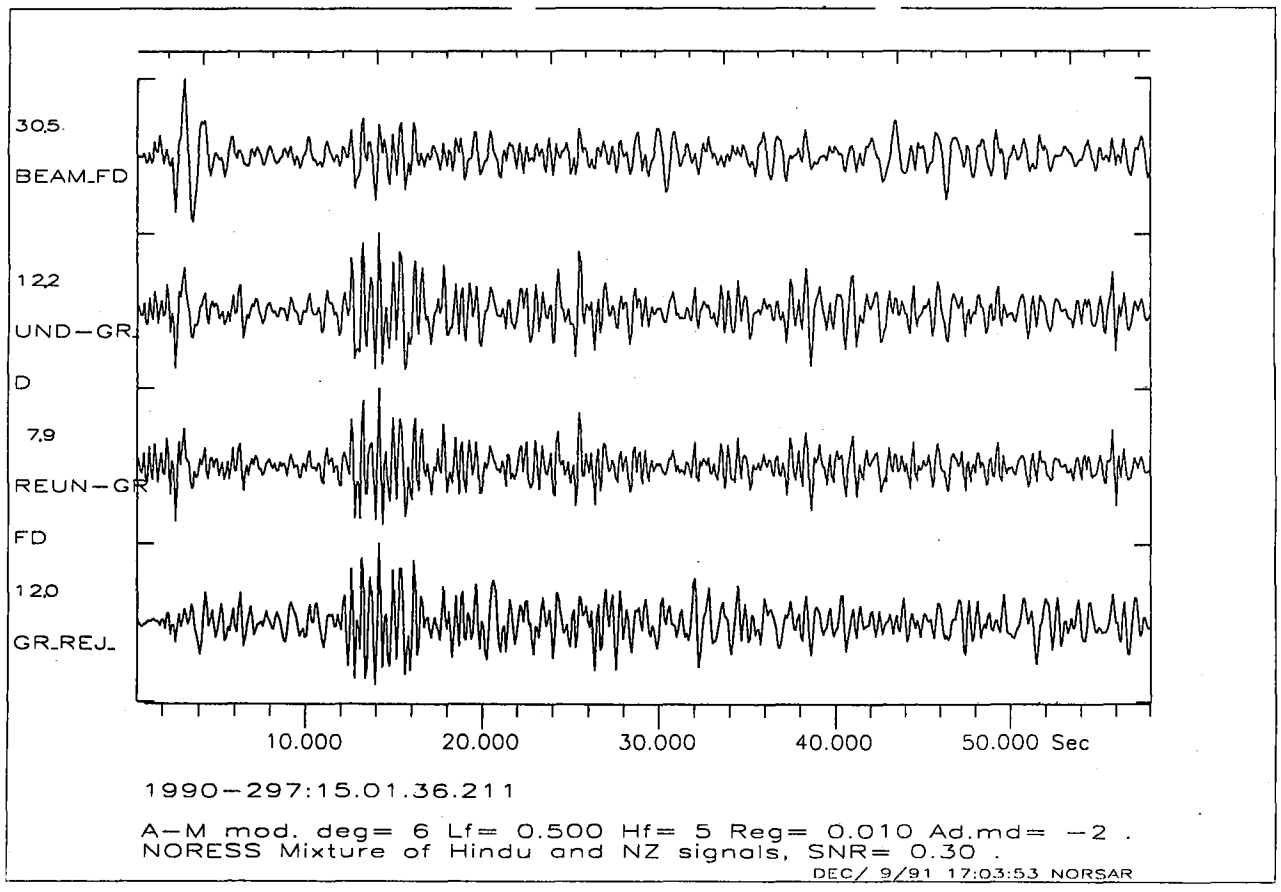

Fig. 7.3.4c. Traces 1-4 correspond to traces 1-4 of Fig. 7.3.4b, but the SNR of the signal is now raised from 0.1 to 0.3. We see that the self-adaptive optimal group filter provide results comparable to the spatial rejection group filter. However, the self-adaptive optimal group filter does not require any information on the slowness or azimuth of the interfering wavetrain.

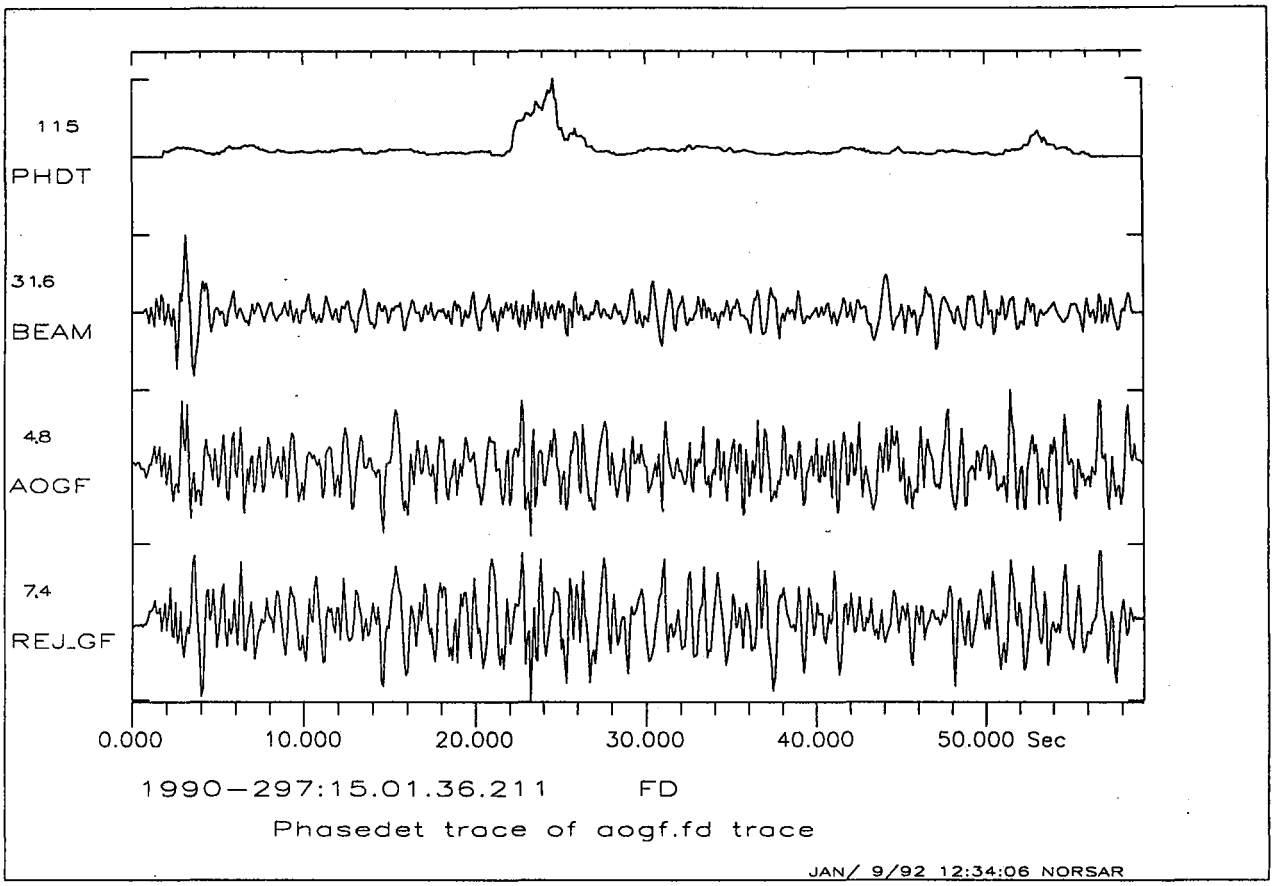

Fig. 7.3.5. Detector statistics from the adaptive optimal phase detector applied to the output from the self-adapted optimal group filter (trace no. 3). Trace no. 2 shows the conventional beam and trace no. 4 shows the spatial rejection group filter output. We see that although the signal (arriving at 21 seconds) is not clearly identified on any of the traces, the adaptive optimal group filter gives us convincing evidence of the presence of a signal.

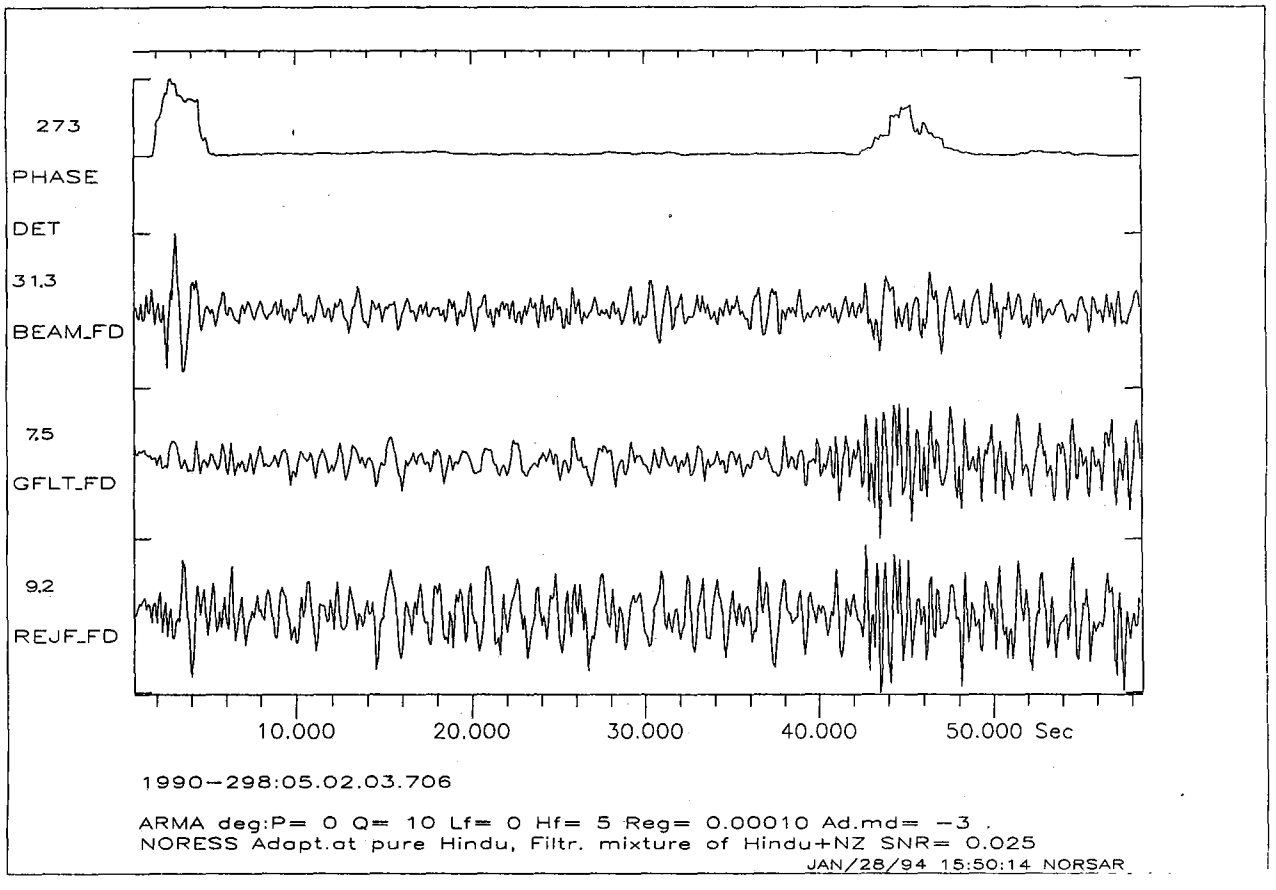

Fig. 7.3.6. Figure illustrating a combined procedure for detecting and extracting a signal with known slowness and azimuth. The signal was set to arrive 41 seconds after the onset of the interfering event, and had a SNR of 0.2. A conventional beam was steered with delays corresponding to the slowness and azimuth of the signal (trace no. 2), and the adaptive optimal phase detector was applied to this conventional beam (trace no. 1). The signal arrival was identified at 41 seconds. The group filter was adapted to the interval 0-39 seconds, and the output from the adaptive optimal group filter is shown in trace no. 3. The signal is now clearly extracted. For comparison the output from the spatial rejection group filter is shown in trace no. 4, but it should be noted that this filter cannot be implemented when information on the interfering event is unknown.